



Cite this: *J. Mater. Chem. B*, 2019,
7, 4066

DOX-assisted functionalization of green tea polyphenol nanoparticles for effective chemo-photothermal cancer therapy

Xiangyu Chen,^{†ab} Zeng Yi,^{ID †ab} Guangcan Chen,^{ID ab} Xiaomin Ma,^{ID ab} Wen Su,^{ID ab} Xinxing Cui^{ab} and Xudong Li ^{ID *ab}

Recently, chemo-photothermal cancer therapy has drawn more and more attention due to its non-invasiveness, low adverse effects and high therapeutic efficiency. Green tea catechins (GTC) including (–)-epigallocatechin-3-gallate (EGCG) are a kind of natural polyphenolic compounds with antitumor activity. In this work, we fabricated nanoparticles loaded with doxorubicin hydrochloride (DOX) and coordinated with Fe(III) for effective chemo-photothermal cancer therapy in which, in a dual role, DOX provided the chemotherapeutic effect and also assisted in achieving nanoparticles with photothermal properties. The GTC nanoparticles (GTCs) were obtained from EGCG and polyethylenimine modified by poly(ethylene glycol) (PEI-PEG) in the presence of formaldehyde. The anticancer drug DOX was encapsulated in GTCs to prepare DOX@GTCs nanoparticles by electrostatic and π - π stacking interactions. After simply mixing with FeCl₃ solutions, EGCG-Fe(III) networks successfully emerged to give nanoparticles with photothermal capacity. *In vitro* experiments indicated that the prepared DOX@GTCs and DOX@GTCs-Fe nanostructures could be effectively internalized into HT-29 cells and that DOX@GTCs-Fe could destroy these cancer cells by hyperthermia in comparison with DOX@GTCs. The animal experiments demonstrated that tumors of mice injected intravenously with both groups of nanoparticles could be effectively inhibited with minimal side effects, confirming their accumulation at tumor sites. Furthermore, the DOX@GTCs-Fe nanoparticles completely ablated the tumor under near-infrared irradiation. Our work indicated that both nanoparticles could achieve targeted drug delivery and that DOX@GTCs-Fe nanoparticles possessed the capability to combine chemo- and photothermal therapy.

Received 18th April 2019,
Accepted 28th May 2019

DOI: 10.1039/c9tb00751b

rsc.li/materials-b

1. Introduction

Cancer is a non-communicable disease, and the first leading cause of death before the age of seventy in the majority of nations of the world.^{1,2} Cancer treatments include clinical surgery, radiotherapy, chemotherapy and phototherapy. Among them, both chemo- and photothermal therapy of cancer have received extensive attention and nanoparticulate pharmaceutical drug delivery systems (NDDSs) play important roles in these cancer treatments. To now, numerous nanoparticles have been investigated as functional carriers of chemotherapeutic agents to improve their therapeutic efficiency, which is generally limited by the nonspecific distribution of antitumor drugs, multidrug

resistance in tumors and inevitable side effects.^{3–6} On the other hand, phototherapies involving photothermal and photodynamic therapies have been developed intensively as effective cancer treatment modes due to their non-invasiveness, high selectivity and minimal side effects.^{7–9} Photothermal therapy (PTT), a prospective treatment method for malignant tumors, employs photothermal agents to absorb photo energy and subsequently generates heat for tumor ablation. A mass of diverse nanomaterials such as gold nanoparticles, dopamine nanomaterials, quantum dots and so on have been applied for efficient photothermal cancer therapy.^{10–16} However, due to the tissue depth limitation of light penetration, the cancer treatment effect of PTT is widely confined. As a result, the combination of photothermal therapy and chemotherapy is a potential method to satisfy these desires of cancer therapy.^{17–22}

Plant-derived polyphenols, a secondary metabolite of plants, have attracted increasing attention for the applications of drug delivery, tissue engineering, and surface functionalization,^{23–25} due to their natural biological activities including antioxidant, anti-inflammatory, antimicrobial and anti-tumor activity.^{26,27}

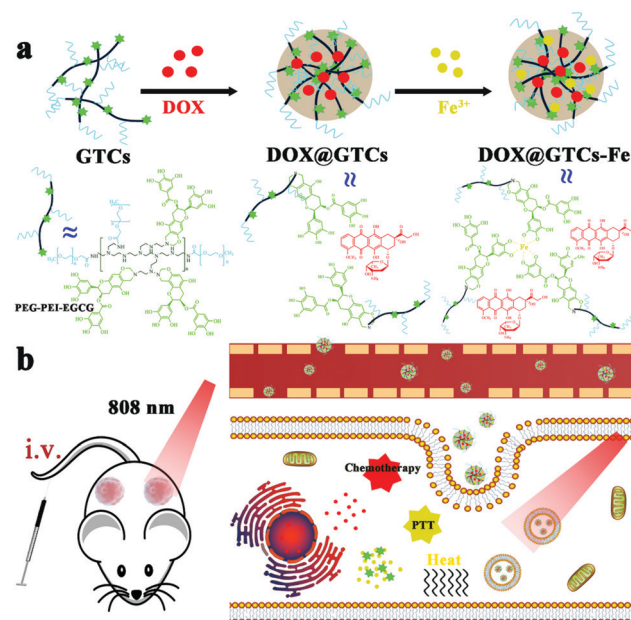
^a Engineering Research Center in Biomaterials, Sichuan University, Chengdu 610064, P. R. China. E-mail: xli20004@yahoo.com; Fax: +86 28 8541 2102; Tel: +86 28 8541 2102

^b National Engineering Research Center for Biomaterials, Chengdu 610064, P. R. China

† These authors contributed equally to this work.

Polyphenols extracted from green tea are a large group of abundant polyphenolic compounds, including (−)-epicatechin (EC), (−)-epicatechin-3-gallate (ECG), (−)-epigallocatechin (EGC), and (−)-epigallocatechin-3-gallate (EGCG). Among them, EGCG is the main active ingredient and has been viewed as an anticancer drug with cancer preventive and therapeutic effects.^{28,29} The majority of studies have demonstrated that EGCG could suppress the promotion of cancers such as breast, colorectal and osteosarcoma as well as leukemia.³⁰ Micelles loaded with doxorubicin hydrochloride (DOX) and EGCG together for cancer treatment could effectively decrease cardio-toxicity and reverse multidrug resistance.³¹ However, many studies have suggested that the biomedical application of EGCG *in vivo* is limited due to its instability, poor bioavailability, low adsorption and rapid metabolism.³² A number of macromolecules such as poly(ethylene glycol) (PEG), keratin, bull serum albumin and chitosan have been applied to improve the stability and enhance the cancer treatment effects of tea catechins.^{33–36} Meanwhile, simply-prepared nanoparticles with pure tea catechins *via* an oxidative coupling reaction are reported to enhance the antitumor activity and alleviate the side effects of DOX in cancer treatment.³⁷ The abundant phenolic hydroxyls of polyphenols endow them not only with high antioxidant properties but also the capability to chelate with metals. DOX-doped ZIF-8 nanoparticles coated with EGCG/Fe networks have been developed as antitumor drug delivery systems with reactive oxygen species (ROS)-responsive properties.³⁸ In addition, nanoparticles coated with tannin acid-Fe(III) have been prepared for photothermal therapy,³⁹ and the photothermal mechanism of the network is due to the strong coordination phenol hydroxyl-metal charge transfer band, which exhibits strong absorption and high heat capacity in the near infrared region.⁴⁰ Despite the recent endeavors to utilize green tea catechins (GTC) with therapeutic effects for NDDSs and metal-phenolic networks for photothermal therapy,^{33,36,37,41} their combination on the basis of green tea polyphenols possessing simultaneously chemo-photothermal capability has not been investigated yet, according to the best of our knowledge. The latest study shows that chemotherapy combined with photothermal performance also exhibits positive results in anti-cancer immunity response.¹⁹ Therefore, the development of EGCG-based nanostructures is promising for chemo- and photothermal therapy of cancer.

In the present work, we reported the preparation, physico-chemical characterization and *in vitro/vivo* biological evaluation of EGCG-based nanostructures with chemotherapeutic and photothermal effects. As shown in Scheme 1a, GTCs were obtained from the covalent assembly of EGCG and polyethylenimine (PEI) modified by PEG (PEI-PEG) in the presence of formaldehyde⁴² and then DOX was loaded by electrostatic and stacking interactions to form DOX@GTCs. Ferric ions were further introduced to endow DOX@GTCs with EGCG-Fe(III) networks. The obtained DOX@GTCs-Fe nanostructures were spheres with a particle size of 159 nm and possessed photothermal effects. After the anticancer activity of DOX@GTCs and DOX@GTCs-Fe was evaluated *in vitro*, both nanoparticles were



Scheme 1 Schematic illustration of (a) covalently-assembled GTCs from EGCG and PEI-PEG to load DOX for DOX@GTCs nanoparticles and further for DOX@GTCs-Fe by chelating with ferric ions, and (b) intravenous injection of both nanoparticles for effective chemo-photothermal cancer treatment under near infrared irradiation.

injected intravenously into tumor-bearing nude mice for assessing the anticancer performance with or without near-infrared irradiation (Scheme 1b). The results showed that both nanoparticles could accumulate at tumor sites and inhibit/ablate the tumor by means of the drug and hyperthermia. The present work would lay a foundation for in-depth understanding of the chemo- and photothermal therapy combination effects of EGCG-based nanomaterials.

2. Experimental section

2.1 Materials

Green tea catechin powder (EGCG ≥ 80%) was obtained from Wuxi Taiyo Green Power Co., Ltd (Jiangsu, China). Branched polyethylenimine (PEI, MW 800), *N*-(3-dimethylaminopropyl)-*N'*-ethylcarbodiimide hydrochloride (EDC-HCl) and *N*-hydroxysuccinimide (NHS) were acquired from Sigma-Aldrich (St. Louis, USA). Methoxypolyethylene glycol 5000 acetic acid (mPEG-COOH, MW 5000) was obtained from Yare Biotechnology (Shanghai, China). Doxorubicin hydrochloride (DOX) was purchased from Dalian Meilun Biological technology (Liaoning, China). Dimethyl sulfoxide (DMSO), formaldehyde and iron(III) chloride hexahydrate (FeCl₃·6H₂O) were purchased from Chengdu Kelong Chemicals (Sichuan, China). Cell counting kit-8 (CCK-8) was purchased from Dojindo Laboratories (Japan). HT-29 and 4T1 cells were purchased from ATCC (USA). Roswell Park Memorial Institute 1640 medium (RPMI-1640), fetal bovine serum (FBS) and penicillin/streptomycin were obtained from Gibco (USA).

2.2 Preparation of DOX@GTCs and DOX@GTCs-Fe nanoparticles (NPs)

Briefly, 500 mg mPEG-COOH, 35 mg EDC, 35 mg NHS and 52 mg PEI were added into 63 mL of DMSO and then the mixture was stirred for 150 min in a water bath at 50 °C. PEG-PEI was obtained by dialyzing the solution in ultrapure (UP) water for 48 h (MWCO 7000). Green tea catechin (100 mg) dissolved in 40 mL UP water was stirred with 2 mL PEG-PEI for 20 min, and then mixed with 42 mL of DOX-HCl solution (1 mg mL⁻¹) at 4 °C for 36 h. After dialyzing (MCWO 7000) against UP water for 48 h, the DOX@GTCs nanoparticles were harvested from the red solution by centrifugation (5000 rpm, 5 min) with UP water three times. Following that, 50, 100 and 200 μL FeCl₃ solution (10 mg mL⁻¹) was separately added into 950, 900 and 800 μL of the re-dispersed aqueous solutions of DOX@GTCs nanoparticles. Theoretically, the introduced concentrations of Fe ion in the 1 mL DOX@GTCs-Fe solution were 0.5, 1.0 and 2.0 mg mL⁻¹. The obtained dark solutions were put at 4 °C overnight and DOX@GTCs-Fe nanoparticles with different ferric ion concentrations (labelled as 0.5, 1.0 and 2.0 mg mL⁻¹) were obtained after washing three times with UP water by centrifugation (5000 rpm, 5 min).

2.3 Characterization

The morphology and size of the samples were observed by transmission electron microscopy (TEM) images obtained from a JEM 1200EX (JEOL, Japan). The surface potential of the particles was measured using a Zetasizer Nano (Malvern, UK). The samples of DOX, DOX@GTCs and DOX@GTCs-Fe were diluted with UP water or DMSO to achieve the equivalent DOX dose. The UV-vis spectra of the solution were obtained using a U-2910 (HITACHI, Japan). The fluorescence spectra of the samples were investigated using a HITACHI F-7000 with an excitation wavelength of 480 nm. The final ferric ion concentration of DOX@GTCs-Fe nanoparticles with different introduced concentrations of Fe³⁺ (0.5, 1.0 and 2.0 mg mL⁻¹) was measured by atomic absorption spectrometry (AAS). To study the photothermal performance of DOX@GTCs-Fe, photothermal evaluation was performed using laser irradiation at 808 nm. 1 mL solutions containing DOX@GTCs-Fe with different ferric ion introduced concentrations were prepared in quartz glass cuvettes at room temperature. With irradiation at 2.5 W cm⁻², the temperature variation of these solutions was recorded once per minute by an infrared thermal imaging camera (CEM DT-980, China). In addition, the temperature of the solutions was measured once every 30 seconds with a mercury thermometer during the heating process, and the solution was placed without irradiation at room temperature for cooling. Finally, the heating/cooling process was repeated three times with the same procedure. Among them, the DOX@GTCs-Fe nanoparticles at a Fe ion introduced concentration of 2 mg mL⁻¹ were chosen for subsequent DOX release, cell and animal experiments.

2.4 In vitro DOX release behaviors of DOX@GTCs and DOX@GTCs-Fe NPs

The drug release profiles of DOX@GTCs and DOX@GTCs-Fe were investigated in phosphate buffer (PBS) at pH = 7.4 and 5.0.

Briefly, 2 mL of DOX@GTCs and DOX@GTCs-Fe solutions (200 μg mL⁻¹) were put into dialysis bags (MCWO 1400 D) and these bags were immersed in PBS solution with pH = 7.4 and 5.0. At determined time points, the solution was taken out for measuring the DOX fluorescence by fluorescence spectrophotometry and equal fresh solution was added immediately.

2.5 Intracellular uptake and *in vitro* cytotoxicity of DOX@GTCs and DOX@GTCs-Fe nanostructures

HT-29 cells were cultured in RPMI-1640 complete medium (500 mL RMPI-1640 medium mixed with 50 mL FBS and 5 mL penicillin/streptomycin solution) under a humidified atmosphere (95% air, 5% CO₂) at 37 °C. To study cancer cell endocytosis of DOX@GTCs and DOX@GTCs-Fe nanoparticles, HT-29 cells were seeded into confocal dishes with a density of 1 × 10⁵ cells per dish for 24 h-incubation. After removing the culture medium, the cells were treated with DOX, DOX@GTCs and DOX@GTCs-Fe (DOX-equivalent dose: 10 μg mL⁻¹) for 0.45 or 3.5 h. After washing three times with PBS, the cells were stained with Hoechst 33342 (3 μg mL⁻¹) for confocal laser scanning microscopy (CLSM) observation. For the flow cytometry experiment, 4T1 cells were seeded into 6 well cell culture plates at a density of 1 × 10⁶ cells per well and after incubation of 24 h, DOX, DOX@GTCs and DOX@GTCs-Fe were respectively added into the wells. The fluorescence intensity of 1 h and 6 h co-incubation was measured at 670 nm using a BD Accuri C6.

CCK-8 assays of HT-29 cells were executed for evaluating the cytotoxicity of DOX@GTCs and DOX@GTCs-Fe. The cells were seeded into 96-well plates with a density of 5 × 10³ cells per well for 24 h, and treated with DOX@GTCs and DOX@GTCs-Fe nanoparticles at a dose of DOX-equivalents of 40, 20, 10, 5, 2.5, 1.25 and 0.625 μg mL⁻¹. After incubation with these nanoparticles for 24 h, the culture medium was removed from each well, and the wells were washed three times with PBS. Then 100 μL of fresh culture medium containing 10% CCK-8 was added into each well, and the optical density (OD) was measured at 450 nm after 2 h of incubation. The cell viability was calculated on the grounds of the equation: Cell viability (%) = (OD_{Sample} - OD_{Background})/(OD_{Control} - OD_{Background}) × 100%. To investigate the photothermal-induced cell death of DOX@GTCs-Fe, the CCK-8 assay was performed again. Some procedures of this process were changed as follows: the HT-29 cells seeded in the 96-well plates were treated with DOX@GTCs-Fe for 2 h. After the cells were exposed to the 808 nm laser (2.5 W cm⁻²) for 5 min at 37 °C, the culture medium of each well was removed and fresh medium was added. Following incubation of 22 h, the CCK-8 assay was performed and the cell viability was calculated according to the aforementioned formula.

2.6 *In vivo* antitumor efficiency of DOX@GTCs-Fe nanoparticles

All the living animal studies were performed in obedience with the relevant laws and institutional guidelines and approved by the ethics committee of Sichuan University. BALB/c male nude mice (4–7 weeks old) were obtained from Chengdu DaShuo Biological Technology Co, Ltd (Sichuan, China). HT-29 cells (5 × 10⁶) were

inoculated into the left/right hind leg of each mouse to establish an animal tumor xenograft model. When the volume of both tumors reached $\sim 100 \text{ mm}^3$, the mice were randomly divided into four groups ($n = 5$), and treated intravenously with glucose (Control, Control IR), DOX, DOX@GTCs, and DOX@GTCs-Fe (DOX@GTCs-Fe, DOX@GTCs-Fe IR) at 1.5 mg kg^{-1} DOX equivalent dose *via* the tail vein every three days. Among them, the tumors at the left side of each mouse in the groups of glucose and DOX@GTCs-Fe were irradiated for 5 min with an 808 nm laser (5 W cm^{-2}) at 6 h after the injection, and the tumors were labelled as Control IR and DOX@GTCs-Fe IR, respectively. The tumor volume and body weight were measured every three days. The tumor volume (V) was calculated as tumor volume = $1/2 \text{ length} \times (\text{width}^2)$. After treatment of fifteen days, the nude mice were sacrificed and the tumors as well as major organs (heart, liver, spleen, lungs and kidneys) of each mouse were collected for histological (hematoxylin–eosin staining, H&E) and immune-histochemical (Ki-67) analyses.

2.7 Statistical analysis

Two-way ANOVA and one-way ANOVA of Dunnett's multiple comparisons test were applied for the statistical significance test. There was a significance difference when the p value was lower than 0.05.

3. Results and discussion

3.1 Physicochemical properties of DOX@GTCs and DOX@GTCs-Fe NPs

The covalent assembly of EGCG with PEI-PEG gave rise to GTCs for the preparation of both DOX@GTCs and DOX@GTCs-Fe nanoparticles. For the latter, a series of Fe^{3+} concentrations were applied to form EGCG-Fe(III) networks among the structure of DOX@GTCs. Typical TEM images of GTC, DOX@GTCs and DOX@GTCs-Fe nanoparticles are shown in Fig. 1a, b and c, respectively. It is evident that the three types of nanoparticles were spherical and the particle size of both DOX@GTCs and DOX@GTCs-Fe visibly increased in comparison with that of GTCs, manifesting that the introduction of DOX to the GTC solution in the absence and presence of ferric ions would promote the functionalization of green tea polyphenol nanoparticles. The functional role of DOX embodied not only providing the anticancer activity but also facilitating obtaining stable nanoparticles. In the preparation of functional nanoparticles, direct collection of solid nanoparticles from GTC solutions containing ferric ions was not successful. In fact, EGCG-metallic complexation was reported to catalyze oxidative polymerization while the formation of an EGCG-Fe or tannic acid-Fe network was used to coat nanoparticles to give ROS-responsiveness or photothermal features.^{23,38,39} DOX is an aromatic compound, and easily forms a steady conjugated system with EGCG, propitious to form DOX-containing objects. The further variation of particle size between DOX@GTCs and DOX@GTCs-Fe can probably be attributed to the metal-phenolic networks derived from EGCG and iron.^{37,43} One hundred

particles were randomly selected from the obtained TEM images, and their sizes were measured. The distribution data of GTC, DOX@GTCs and DOX@GTCs-Fe nanoparticles are given in Fig. 1a1, b1 and c1. The average size was 50 nm for GTC, 128 nm for DOX@GTCs and 159 nm for DOX@GTCs-Fe nanoparticles. The difference in size of 31 nm between DOX@GTCs and DOX@GTCs-Fe arises from the addition of 2 mg mL^{-1} Fe(III) ions for preparing the DOX@GTCs-Fe nanoparticles, indicative of the existence of competition between DOX loading and Fe-chelation. The higher number of EGCG-Fe(III) coordinations was believed to give a more loose structure. The UV absorption spectra are given in Fig. 1d. The characteristic absorption peaks of EGCG and DOX were located respectively at 280 nm and 480 nm. In the spectrum of DOX@GTCs, both of the characteristic adsorption peaks appeared, testifying that DOX and EGCG existed in DOX@GTCs. The slight red shift of the DOX characteristic adsorption was recorded, suggesting the existence of $\pi-\pi$ stacking interactions in the loading of DOX. This was also the case in DOX@GTCs-Fe nanoparticles. As demonstrated in Fig. 1e, the zeta potential of GTC and DOX@GTCs nanoparticles was $-32.6 \pm 0.57 \text{ mV}$ and $-6.57 \pm 0.46 \text{ mV}$, verifying that the loading of negatively charged DOX into GTCs also included electrostatic interactions. In addition, the zeta potential of DOX@GTCs-Fe nanoparticles was $+31.27 \pm 0.23 \text{ mV}$, which was superior in a targeted drug delivery system *in vivo* over the negatively charged nanoparticles.⁴⁴ The fluorescence emission spectrum was further employed to explore the interactions of DOX loading in DOX@GTCs and DOX@GTCs-Fe nanostructures, and these spectra were recorded in aqueous and DMSO solution. The fluorescence intensity of DOX@GTCs and DOX@GTCs-Fe in aqueous solution (Fig. 1f) was lower than that of DOX, indicating that the fluorescence of DOX was quenched because of the electronic energy transfer. In DMSO solution (Fig. 1g), the fluorescence intensity of DOX@GTCs and DOX@GTCs-Fe was stronger than that of Fig. 1e, which demonstrated the DOX was successfully loaded into the GTCs.

3.2 Photothermal properties and DOX release behaviors of DOX@GTCs and DOX@GTCs-Fe NPs

For various applications of polyphenol, its capacity to chelate metal ions has gained more and more attention.^{45–49} Metal-polyphenolic networks have been prepared by a facile, rapid and green method from different polyphenols such as dopamine, gallic acid, pyrocatechol, tannin acid and so on.^{50–52} Among them, tannin acid-Fe(III) networks were shown to exhibit good photothermal capability for photo-induced cancer therapy.^{39,40} Here, we studied the photothermal performance of DOX@GTCs-Fe with EGCG-Fe(III) networks. In photo-induced cancer therapy, near infrared light is a suitable candidate for irradiation due to its deep tissue penetration ability and minimal damage to normal tissue.⁵³ Therefore, the temperature changes of DOX@GTCs-Fe at a varying ferric ion introduced concentration (0, 0.5, 1.0 and 2.0 mg mL^{-1}) were investigated under irradiation at 808 nm with a laser power of 2.5 W cm^{-2} . The solution at a concentration of 0 mg mL^{-1} was set as a control. The infrared thermal images show the temperature variation within 5 min (Fig. 2a).

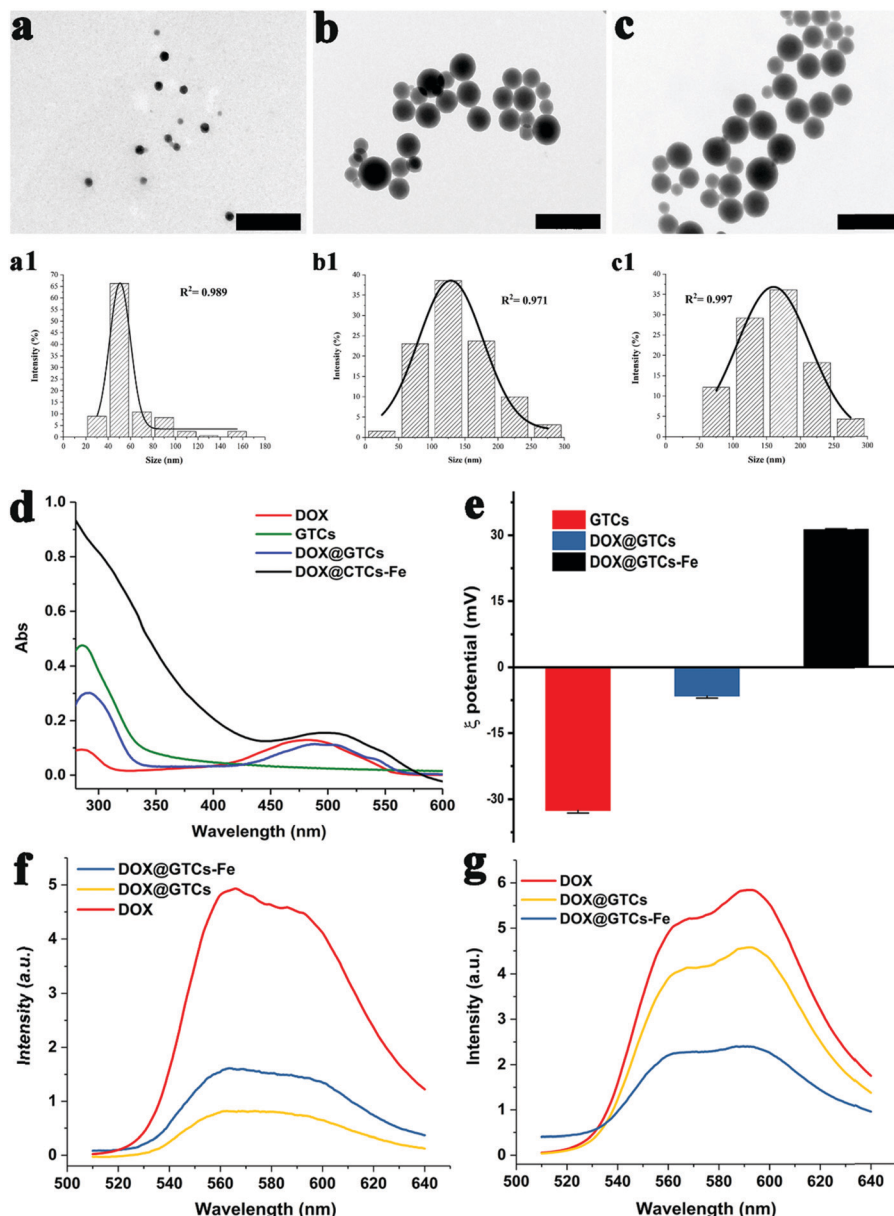


Fig. 1 TEM images of (a) GTCs, (b) DOX@GTCs and (c) DOX@GTCs-Fe. Scale bar is 500 nm. The statistical analysis of the particle-size of (a1) GTCs, (b1) DOX@GTCs and (c1) DOX@GTCs-Fe from TEM photographs by image analysis software. (d) The UV-vis spectrum of DOX, GTCs, DOX@GTCs and DOX@GTCs-Fe. (e) The zeta potential of GTCs, DOX@GTCs and DOX@GTCs-Fe. The fluorescence emission spectrum of DOX, DOX@GTCs and DOX@GTCs-Fe in (f) aqueous and (g) DMSO solution.

Compared with the control group, the groups at Fe(III) introduced concentrations of 0.5, 1.0 and 2.0 mg mL⁻¹ exhibited a trend in the elevation of temperature. Measured by AAS, the ultimate ferric ion concentrations of these samples were 0.40, 0.80 and 1.62 mg mL⁻¹. With increasing the Fe(III) concentration, the temperature of DOX@GTCs-Fe steadily rose, finally reaching a maximum temperature of 41 °C. These results confirmed that the EGCG-Fe(III) networks in DOX@GTCs-Fe could effectively adsorb light to generate heat, indicating that the DOX@GTCs-Fe nanoparticles have potential as photothermal agents to kill cancer cells at specific tumor sites by their photothermal capacity. To further study the photothermal effect of DOX@GTCs-Fe, the time-temperature curve

is shown in Fig. 2b. Among all the groups, the DOX@GTCs-Fe NPs prepared in the group of 2.0 mg mL⁻¹ Fe(III) showed the highest increment in temperature variation, in accordance with the data given in Fig. 2a. The maximum temperature change for 5 min was 10 °C and appeared in the group of 2.0 mg mL⁻¹. It is evident that according to the results of Fig. 2a and b, the group of 2.0 mg mL⁻¹ exhibited the optimal photothermal effects within the four groups of DOX@GTCs-Fe NPs. It is probably because the highest number of coordination structures existed in the nanoparticles prepared at the highest Fe(III) concentration. The DOX@GTCs-Fe NPs with the 2.0 mg mL⁻¹ Fe(III) introduced concentration were selected for subsequent cell and animal experiments.

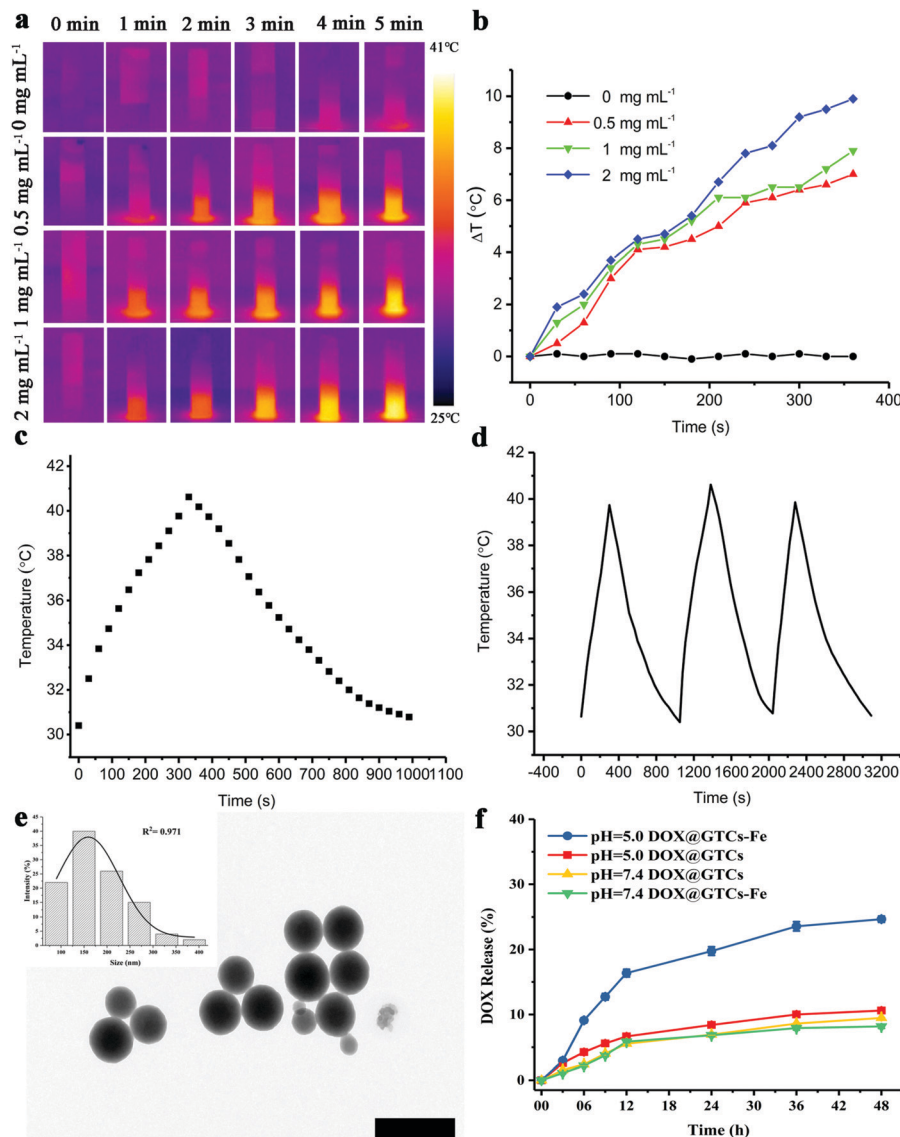


Fig. 2 (a) Thermal images and (b) temperature variation curves within 5 min of DOX@GTCs-Fe with different ferric concentrations upon 808 nm laser irradiation (2.5 W cm^{-2}). (c) Temperature rising/falling curve with/without 808 nm irradiation. (d) Temperature change within three times of the cyclic heating/cooling process. (e) TEM image of the DOX@GTCs-Fe nanoparticles with irradiation of three times and the inset is the size distribution data of these particles. Scale bar is 500 nm. (f) DOX release profiles of DOX@GTCs and DOX@GTCs-Fe nanoparticles in PBS at pH = 7.4 and 5.0.

The temperature rising/falling curve with/without 808 nm irradiation is shown in Fig. 2c. The temperature was shown to go up rapidly with the laser irradiation at the beginning, and then down slowly to room temperature without irradiation for 10 min. The temperature change within three times of the cyclic heating/cooling process was used to investigate the durability of the photothermal properties. The results in Fig. 2d confirmed that the DOX@GTCs-Fe had good photostability. The size distribution of particles after the last time of the heating/cooling process was obtained from TEM images, and the statistical data showed that the particle size (161 nm) was slightly changed compared with that before irradiation (159 nm), further indicating the photostability of DOX@GTCs-Fe NPs after multiple irradiation cycles (Fig. 1c, c1 and 2e). As shown in Fig. 2f,

the DOX release from DOX@GTCs and DOX@GTCs-Fe NPs was detected in PBS with different pH (7.4 or 5.0). At pH = 7.4, the DOX release from the DOX@GTCs and DOX@GTCs-Fe NPs was 10% and 8% after 48 h. The relatively low drug release is due to the strong binding force between PEG and EGCG, which makes it difficult for drugs to diffuse from the nanoparticles into the release media, and a similar phenomenon has been reported in other literature.³⁶ With the pH decreased to 5.0, a part of the hydroxyl groups were protonated, leading to destabilization of coordinate-bonds and disassembly of the nanoparticles.⁵⁴ The cumulative release rate of DOX in the DOX@GTCs and DOX@GTCs-Fe groups increased to 12% and 26%, respectively. The DOX release ability of DOX@GTCs-Fe was immensely enhanced, showing that the DOX@GTCs-Fe NPs could exhibit a

pH-responsive property for the controlled release of DOX due to the pH-sensitivity of metal-phenolic networks.^{55,56}

3.3 Cellular uptake and cytotoxicity of DOX@GTCs and DOX@GTCs-Fe NPs

The cellular uptake of DOX, DOX@GTCs and DOX@GTCs-Fe was investigated by determining the fluorescence intensity using CLSM and flow cytometry. DOX, an amphipathic small

molecule drug, could readily get into cells by free diffusion. After incubation for 0.45 h, the red fluorescence of DOX was also observed in the group of DOX@GTCs and DOX@GTCs-Fe, although weaker than that of the DOX group, still indicating that cancer cells could effectively ingest the DOX@GTCs and DOX@GTCs-Fe nanoparticles (Fig. 3a). Comparatively, the fluorescence of the DOX@GTCs-Fe group was further weaker than that of the DOX@GTCs group, indicating that

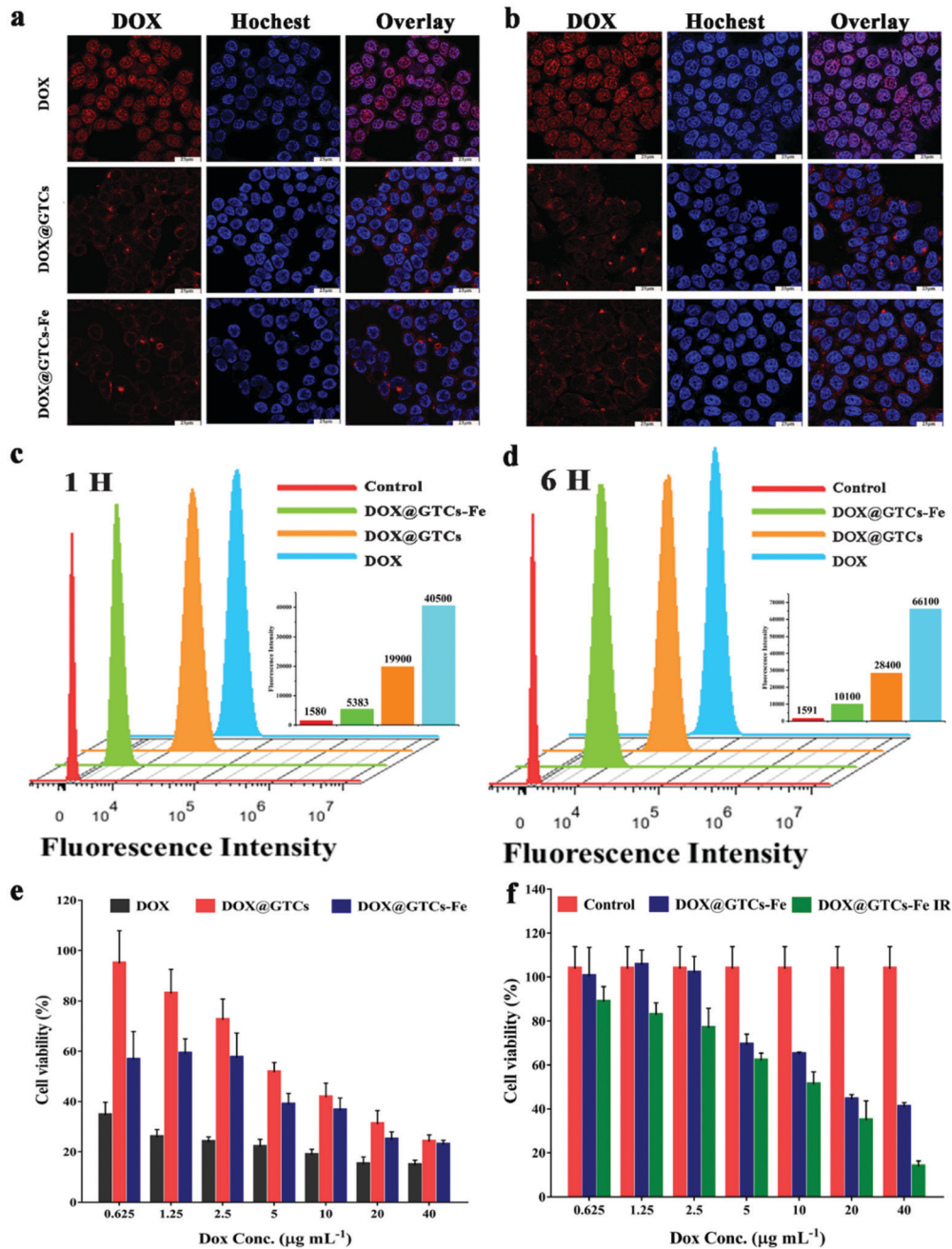


Fig. 3 CLSM images of HT-29 cells incubated with free DOX, DOX@GTCs and DOX@GTCs-Fe (equivalent dose of DOX: $10 \mu\text{g mL}^{-1}$) for (a) 0.45 h and (b) 3.5 h. The nuclei stained with Hoechst 33342 were blue, and the red fluorescence resulted from free DOX. Scale bar: $25 \mu\text{m}$. Flow cytometry analysis of 4T1 cells incubated with DOX, DOX@GTCs and DOX@GTCs-Fe for (c) 1 h and (d) 6 h and the insets are the corresponding fluorescence intensity. (e) Photothermal cytotoxicity of DOX@GTCs and DOX@GTCs-Fe against HT-29 cells after incubation for 24 h. (f) Cell viability of HT-29 cells irradiated at 808 nm with a power density of 2.5 W cm^{-2} for 5 min after incubating with DOX@GTCs-Fe for 2 h. Cells without irradiation were set as the Control.

the relatively slow release of DOX was probably due to the positive surface of DOX@GTCs-Fe nanoparticles.⁵⁷ With the extension of the incubation time to 3.5 h, the red fluorescence in the groups of DOX@GTCs and DOX@GTCs-Fe enhanced, specifying that more nanoparticles were internalized by HT-29 cells and a larger amount of DOX was subsequently released (Fig. 3b). For further explore the intracellular uptake of these nanoparticles, flow cytometry was employed. As shown in Fig. 3c, the fluorescence intensity of the DOX@GTCs group was higher than that of the DOX@GTCs-Fe group, corresponding to the results of CLSM. With increasing the co-incubation time of cancer cells with nanoparticles, the DOX fluorescence intensity of all the groups was enhanced but the red fluorescence of DOX@GTCs-Fe was still weaker than that in the DOX@GTCs group, showing the same results as Fig. 3b (Fig. 3d). To appraise quantitatively the anticancer capability of DOX@GTCs and DOX@GTCs-Fe, CCK-8 assays were performed on HT-29 cells and the cell viability was counted using

the GraphPad Prism software. The HT-29 cells were treated with DOX, DOX@GTCs and DOX@GTCs-Fe of various concentrations ranging from $0.625 \mu\text{g mL}^{-1}$ to $40 \mu\text{g mL}^{-1}$ for 24 h, and their inhibitory effects against the cell proliferation were investigated. The results showed that the inhibition ability of DOX@GTCs enhanced with increasing DOX concentration and in the DOX@GTCs-Fe group the same positive relationship emerged with concentrations ranging from $2.5 \mu\text{g mL}^{-1}$ to $40 \mu\text{g mL}^{-1}$ (Fig. 3e). In general, the cytotoxicity of DOX@GTCs and DOX@GTCs-Fe against cancer cells was not as strong as that of free DOX, possibly arising from the relatively moderate release of DOX. However, the cytotoxicity of DOX@GTCs-Fe against HT-29 cells was enhanced upon irradiation at 808 nm (Fig. 3f). Compared with the group of DOX@GTCs-Fe without light, the cancer inhibition capability of that with light was obviously improved, indicating the photothermal effect of DOX@GTCs-Fe could suppress tumor cell growth *in vitro*.

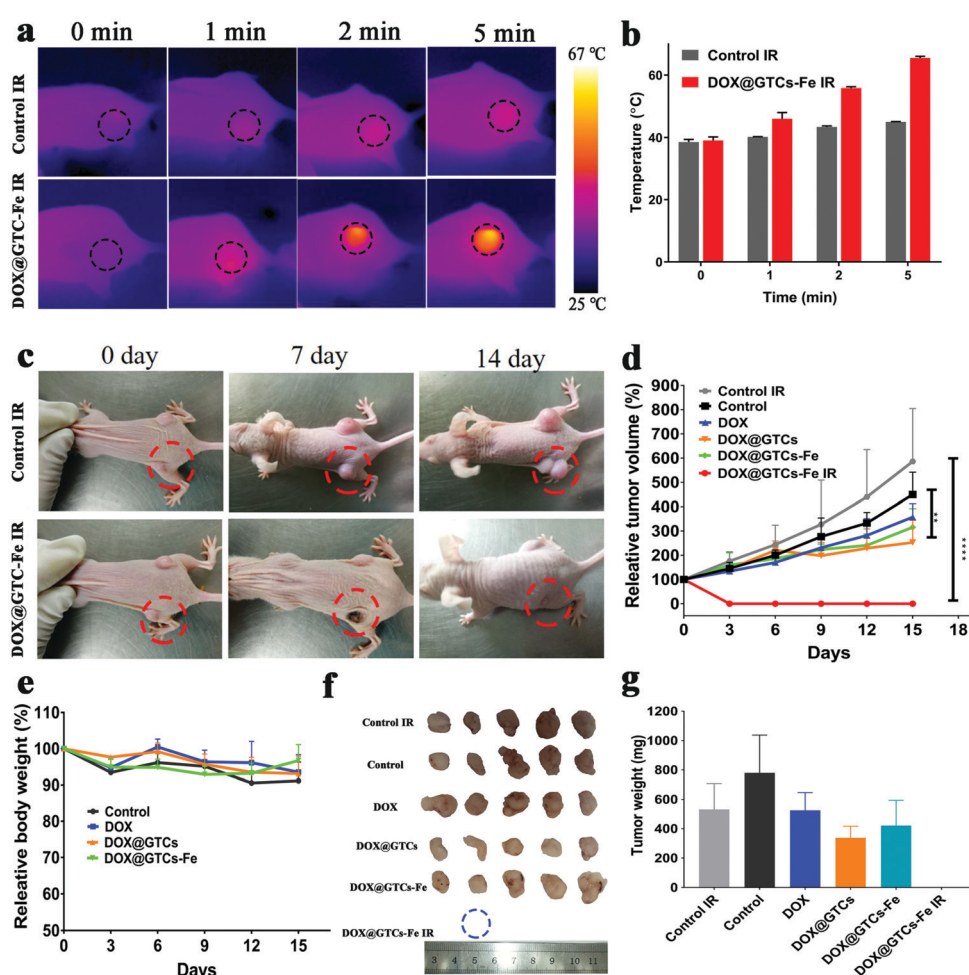


Fig. 4 *In vivo* antitumor effect of the HT-29 tumor-bearing BALB/c nude mice. (a) The IR images and (b) the tumor temperature change of mice irradiated at 808 nm for 1, 2 and 5 min after being treated with DOX@GTCs-Fe. (c) The digital photographs of nude mice after photothermal therapy (left hind leg). (d) The relative tumor volume of mice from the groups of the Control, Control IR, DOX, DOX@GTCs and DOX@GTCs-Fe and DOX@GTCs-Fe IR. (e) The relative body weight variation of mice injected intravenously with glucose (Control), DOX, DOX@GTCs and DOX@GTCs-Fe. Data are shown as means \pm standard deviation. ($n = 5$, ordinary two-way ANOVA with Tukey's multiple comparison test: ** $p < 0.01$, *** $p < 0.0001$). (f) Images and (g) weight of isolated tumors collected from mice of each group.

3.4 In vivo antitumor performance of DOX@GTCs and DOX@GTCs-Fe NPs

On the basis of the antitumor performance *in vitro* of DOX@GTCs and DOX@GTCs-Fe nanoparticles, the *in vivo* evaluation of their antitumor activity was further studied. BALB/C nude mice xenograft models were obtained by the subcutaneous injection of HT-29 cells, and these mice with tumors in both left and right flanks were randomly divided into four groups. After these tumors reached about 100 mm³, the mice were respectively treated with glucose (Control), DOX, DOX@GTCs, and DOX@GTCs-Fe (DOX-equivalent dose: 1.5 mg kg⁻¹) every three days by tail vein injection. In addition, photothermal therapy was performed on the left tumor of the Control and DOX@GTCs-Fe groups at 6 h after the first injection. As shown in Fig. 4a, the change of the tumor temperature during five minutes with the irradiation at 808 nm (5 W cm⁻²) was recorded at 0, 1, 2 and 5 min by infrared thermal image instruments. In comparison with that of the Control group, the tumor temperature of the DOX@GTCs-Fe IR group displayed an escalating trend and the maximum temperature within 5 min was about 62 °C (Fig. 4a and b). As depicted in Fig. 4c, the tumors (dotted line circle) of

the mouse in the Control group kept increasing during treatment of 15 d, but those in the group of DOX@GTCs-Fe IR were effectively decreased and finally ablated, validating the photothermal property of DOX@GTCs-Fe nanoparticles. The tumor volume and body weight were measured every three days for quantitatively studying the capability of DOX@GTCs and DOX@GTCs-Fe nanoparticles to inhibit tumor growth. During the 15 day treatment period, all the treatment groups including DOX, DOX@GTCs, DOX@GTCs and DOX@GTCs-Fe, DOX@GTCs-Fe IR could effectively suppress tumor growth compared with the other Control groups (Fig. 4d). It is worthy to note that this good result was achieved at a relatively low administration dose of DOX (1.5 mg kg⁻¹). The *in vitro* cancer cell inhibition experiments showed that the anticancer efficiency of DOX was superior to the DOX@GTCs and DOX@GTCs-Fe groups, but the *in vivo* tumor growth inhibition of the DOX@GTCs and DOX@GTCs-Fe groups was similar to DOX, demonstrating that these particles were capable of delivering DOX to tumor locations and assuring therapeutic efficacy with slow drug release and long circulation *in vivo*. The results showed that the GTC NPs could be set as

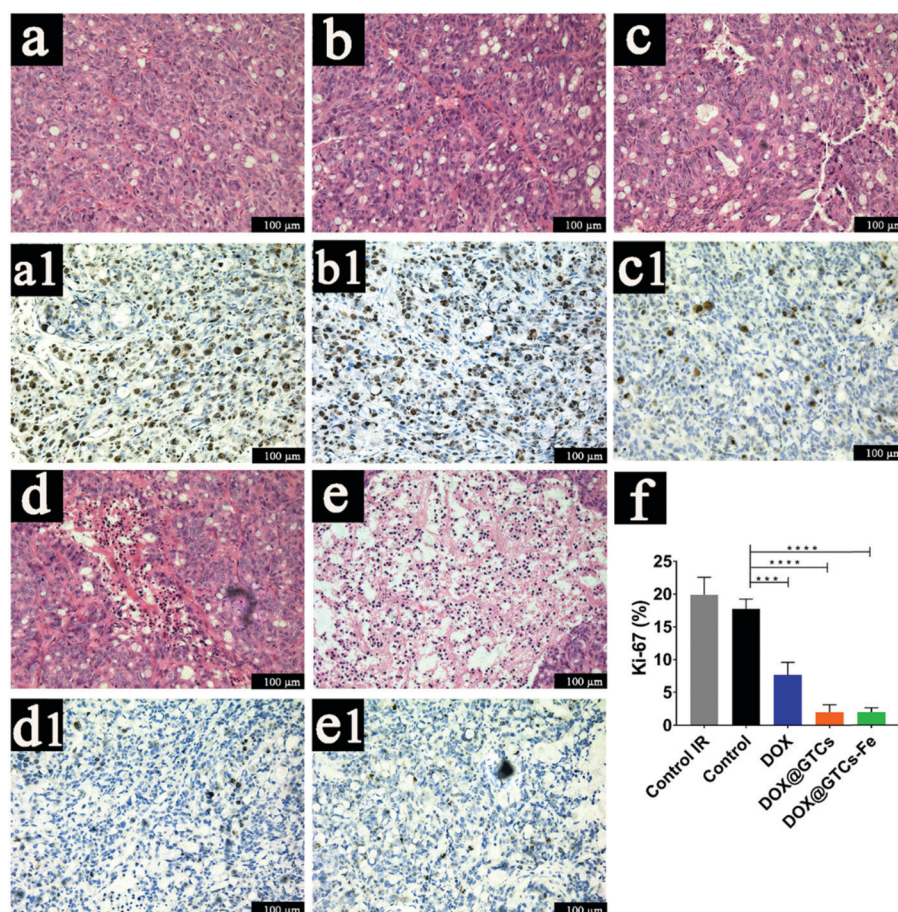


Fig. 5 H&E staining images of the tumor sections from the treatment of (a) Control IR, (b) Control, (c) DOX, (d) DOX@GTCs, and (e) DOX@GTCs-Fe and the relevant Ki-67 immuno-histochemical images (a1, b1, c1, d1 and e1). Scale bar is 50 μm. (f) The Ki-67 density of images from each group calculated from the ratio of the Ki-67 positive area to the total area using ImageJ software ($n = 5$, ordinary one-way ANOVA with Dunnett's multiple comparison test: *** $p < 0.0001$).

nanocarriers for efficient drug delivery systems. Fig. 4d shows that the tumors in the mice of the DOX@GTCs-Fe IR group dramatically disappeared, indicative of the combination effect of chemotherapy and photothermal therapy. The relative body weight in all four groups of mice did not exhibit an obvious decrease, confirming the good biocompatibility of DOX@GTCs and DOX@GTCs-Fe. After the treatment, solid tumors from sacrificed mice of each group were collected and weighed. Compared with the Control IR group, DOX@GTCs-Fe nanoparticles together with near-infrared irradiation obviously ablated the tumor, which was in accordance with the changes in tumor volume over time (Fig. 4f and g).

The tumors and main organs including the heart, liver, spleen, lung and kidney were collected for H&E and immunohistochemical staining from the sacrificed mice of all these groups. As shown in Fig. 5, the tumor tissue from the Control IR group presented dense tumor cells with few necrotic cells, verifying that laser treatment alone at a power density of 5 W cm^{-1} could not prevent the uncontrollable proliferation of cancer cells and ultimately achieve tumor ablation. However, the group of DOX@GTCs-Fe IR exhibited tumor elimination ability during the 15 day treatment period, illustrating the photothermal antitumor effect of DOX@GTCs-Fe nanoparticles and the combination of photothermal therapy and chemotherapy

would exert better antitumor capability compared with single-mode cancer treatment (Fig. 4d and f). The tumor tissues of the DOX@GTCs and DOX@GTCs-Fe showed large areas of tumor necrosis compared with the other three groups, which indicated that DOX could be delivered to tumor sites by GTCs and then destroyed cancer cells by the effects of chemotherapy (Fig. 5d and e). The nuclear protein Ki-67 is one of the standard markers of tumor cellular proliferation.⁵⁸ As depicted in Fig. 5f, the groups of DOX@GTCs and DOX@GTCs-Fe indicated the lower level of Ki-67 positive cells in comparison with the Control, Control IR and DOX groups, demonstrating that these nanocomposites could efficiently hinder tumor cell proliferation. The heart slice of the DOX group still showed obvious myocardial lesions even at low dose, exhibiting tough DOX-induced cardiotoxicity. It is noteworthy that no significant toxicity was shown in the heart sections of the DOX@GTCs and DOX@GTCs-Fe groups, which probably was because of the GTC nanoparticles containing EGCG.^{37,59} Moreover, there is no significant toxicity in the other organ tissues (liver, spleen, lung and kidney) of DOX@GTCs and DOX@GTCs-Fe in comparison with the Control and DOX groups, confirming the minimal side effects of DOX@GTCs and DOX@GTCs-Fe nanoparticles (Fig. 6). Overall, *in vivo* experiments demonstrated that both groups of nanoparticles were capable of achieving targeted drug delivery and that DOX@GTCs-Fe

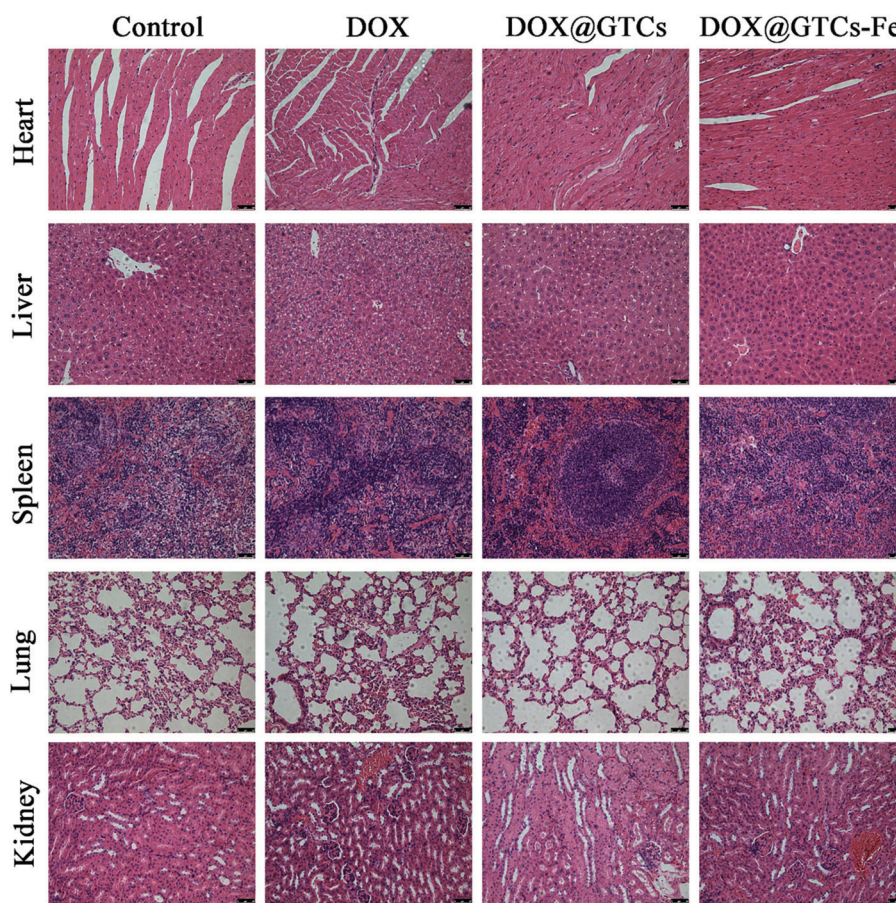


Fig. 6 Histological analyses of H&E stained slices of main organs from tumor-bearing mice injected with DOX, DOX@GTCs and DOX@GTCs-Fe. Scale bar is $100 \mu\text{m}$.

nanoparticles possessed the capability to combine chemo- and photothermal therapy.

4. Conclusions

In summary, EGCG-based nanostructures with chemotherapeutic and photothermal effects were prepared, characterized and evaluated. These nanostructures were achieved on the basis of covalently assembled GTCs with EGCG and PEI-PEG for loading DOX as DOX@GTCs and further chelating with ferric ions as DOX@GTCs-Fe. The DOX added into the GTC solutions assisted in the synthesis of DOX@GTCs and DOX@GTCs-Fe, and acted as the functional component of antineoplastic activity in both nanoparticles. The average size was 128 nm for DOX@GTCs and 159 nm for DOX@GTCs-Fe nanoparticles. The successful loading of DOX was realized by electrostatic and π - π stacking interactions. The formation of EGCG-Fe(III) networks was responsible for the photothermal effects of DOX@GTCs-Fe nanoparticles. *In vitro* cellular experiments confirmed that both nanoparticles exhibited the inhibition of cancer cell proliferation. Under near-infrared irradiation, DOX@GTCs-Fe nanoparticles further had enhanced anticancer activity. *In vivo* experiments indicated that DOX@GTCs and DOX@GTCs-Fe nanoparticles could reach specific tumor sites *via* intravenous injection and suppress tumor growth, along with minimal side effects. The tumors treated with DOX@GTCs-Fe NPs totally disappeared under laser irradiation at 808 nm, probably due to the combination effects of the drug and hyperthermia. The present work not only provides a strategy to make good use of tea polyphenols but also lays a foundation for in-depth understanding of the chemo- and photothermal therapy combination effects of EGCG-based nanomaterials.

Conflicts of interest

The authors declare no competing financial interest.

Acknowledgements

This work was supported by the National Natural Science Foundation of China (No. 51373106, 31872750), the National Key Research and Development Program of China (No. 2016YFC1102700) and the National Basic Research Program of China (No. 2012CB933600).

References

- 1 F. Bray, J. Ferlay, I. Soerjomataram, R. L. Siegel, L. A. Torre and A. Jemal, Global Cancer Statistics 2018: Globocan Estimates of Incidence and Mortality Worldwide for 36 Cancers in 185 Countries, *Ca-Cancer J. Clin.*, 2018, **68**(6), 394–424.
- 2 V. Shanmugam, S. Selvakumar and C. S. Yeh, Near-Infrared Light-Responsive Nanomaterials in Cancer Therapeutics, *Chem. Soc. Rev.*, 2014, **43**(17), 6254–6287.
- 3 X. Yi, K. Yang, C. Liang, X. Zhong, P. Ning, G. Song, D. Wang, C. Ge, C. Chen, Z. Chai and Z. Liu, Imaging-Guided Combined Photothermal and Radiotherapy to Treat Subcutaneous and Metastatic Tumors Using Iodine-131-Doped Copper Sulfide Nanoparticles, *Adv. Funct. Mater.*, 2015, **25**(29), 4689–4699.
- 4 R. Zhang, R. Xing, T. Jiao, K. Ma, C. Chen, G. Ma and X. Yan, Carrier-Free, Chemophotodynamic Dual Nanodrugs Via Self-Assembly for Synergistic Antitumor Therapy, *ACS Appl. Mater. Interfaces*, 2016, **8**(21), 13262–13269.
- 5 Z. Sun, Z. Yi, H. Zhang, X. Ma, W. Su, X. Sun and X. Li, Bio-Responsive Alginate-Keratin Composite Nanogels with Enhanced Drug Loading Efficiency for Cancer Therapy, *Carbohydr. Polym.*, 2017, **175**, 159–169.
- 6 Z. Sun, Z. Yi, X. Cui, X. Chen, W. Su, X. Ren and X. Li, Tumor-Targeted and Nitric Oxide-Generated Nanogels of Keratin and Hyaluronan for Enhanced Cancer Therapy, *Nanoscale*, 2018, **10**(25), 12109–12122.
- 7 L. Cheng, C. Wang, L. Feng, K. Yang and Z. Liu, Functional Nanomaterials for Phototherapies of Cancer, *Chem. Rev.*, 2014, **114**(21), 10869–10939.
- 8 H. Zhu, P. Cheng, P. Chen and K. Pu, Recent Progress in the Development of near-Infrared Organic Photothermal and Photo-dynamic Nanotherapeutics, *Biomater. Sci.*, 2018, **6**(4), 746–765.
- 9 F. Wu, M. Zhang, X. Chu, Q. Zhang, Y. Su, B. Sun, T. Lu, N. Zhou, J. Zhang, J. Wang and X. Yi, Black Phosphorus Nanosheets-Based Nanocarriers for Enhancing Chemotherapy Drug Sensitiveness Via Depleting Mutant P53 and Resistant Cancer Multimodal Therapy, *Chem. Eng. J.*, 2019, **370**, 387–399.
- 10 H. Sekyu, N. Jutaek, J. Sungwook, S. Jaejung, D. Hyunmi and K. Sungjee, Gold Nanoparticle-Mediated Photothermal Therapy: Current Status and Future Perspective, *Nanomedicine*, 2014, **9**(13), 2003–2022.
- 11 X. Liu, N. Huang, H. Li, H. Wang, Q. Jin and J. Ji, Multidentate Polyethylene Glycol Modified Gold Nanorods for *in vivo* near-Infrared Photothermal Cancer Therapy, *ACS Appl. Mater. Interfaces*, 2014, **6**(8), 5657–5668.
- 12 W. Tao, X. Ji, X. Xu, M. A. Islam, Z. Li, S. Chen, P. E. Saw, H. Zhang, Z. Bharwani, Z. Guo, J. Shi and O. C. Farokhzad, Antimonene Quantum Dots: Synthesis and Application as near-Infrared Photothermal Agents for Effective Cancer Therapy, *Angew. Chem., Int. Ed.*, 2017, **56**(39), 11896–11900.
- 13 Y. Liu, K. Ai, J. Liu, M. Deng, Y. He and L. Lu, Dopamine-Melanin Colloidal Nanospheres: An Efficient near-Infrared Photothermal Therapeutic Agent for *in vivo* Cancer Therapy, *Adv. Mater.*, 2013, **25**(9), 1353–1359.
- 14 X. Yao, Z. Tian, J. Liu, Y. Zhu and N. Hanagata, Mesoporous Silica Nanoparticles Capped with Graphene Quantum Dots for Potential Chemo-Photothermal Synergistic Cancer Therapy, *Langmuir*, 2017, **33**(2), 591–599.
- 15 M. Zhang, W. Wang, N. Zhou, P. Yuan, Y. Su, M. Shao, C. Chi and F. Pan, Near-Infrared Light Triggered Photo-Therapy, in Combination with Chemotherapy Using Magnetofluorescent Carbon Quantum Dots for Effective Cancer Treating, *Carbon*, 2017, **118**, 752–764.

- 16 Z. Tian, X. Yao, K. Ma, X. Niu, J. Grothe, Q. Xu, L. Liu, S. Kaskel and Y. Zhu, Metal-Organic Framework/Graphene Quantum Dot Nanoparticles Used for Synergistic Chemo- and Photo-thermal Therapy, *ACS Omega*, 2017, **2**(3), 1249–1258.
- 17 S. Wang, X. Zhao, S. Wang, J. Qian and S. He, Biologically Inspired Polydopamine Capped Gold Nanorods for Drug Delivery and Light-Mediated Cancer Therapy, *ACS Appl. Mater. Interfaces*, 2016, **8**(37), 24368–24384.
- 18 H. Chen, Y. Di, D. Chen, K. Madrid, M. Zhang, C. Tian, L. Tang and Y. Gu, Combined Chemo- and Photo-Thermal Therapy Delivered by Multifunctional Theranostic Gold Nanorod-Loaded Microcapsules, *Nanoscale*, 2015, **7**(19), 8884–8897.
- 19 J. Nam, S. Son, L. J. Ochyl, R. Kuai, A. Schwendeman and J. J. Moon, Chemo-Photothermal Therapy Combination Elicits Anti-Tumor Immunity against Advanced Metastatic Cancer, *Nat. Commun.*, 2018, **9**(1), 1074.
- 20 Y. Wang, G. Wei, X. Zhang, X. Huang, J. Zhao, X. Guo and S. Zhou, Multistage Targeting Strategy Using Magnetic Composite Nanoparticles for Synergism of Photothermal Therapy and Chemotherapy, *Small*, 2018, **14**(12), e1702994.
- 21 F. Wu, M. Zhang, H. Lu, D. Liang, Y. Huang, Y. Xia, Y. Hu, S. Hu, J. Wang, X. Yi and J. Zhang, Triple Stimuli-Responsive Magnetic Hollow Porous Carbon-Based Nanodrug Delivery System for Magnetic Resonance Imaging-Guided Synergistic Photothermal/Chemotherapy of Cancer, *ACS Appl. Mater. Interfaces*, 2018, **10**(26), 21939–21949.
- 22 P. Pei, F. Yang, J. Liu, H. Hu, X. Du, N. Hanagata, S. Zhao and Y. Zhu, Composite-Dissolving Microneedle Patches for Chemotherapy and Photothermal Therapy in Superficial Tumor Treatment, *Biomater. Sci.*, 2018, **6**(6), 1414–1423.
- 23 Z. Chen, C. Wang, J. Chen and X. Li, Biocompatible, Functional Spheres Based on Oxidative Coupling Assembly of Green Tea Polyphenols, *J. Am. Chem. Soc.*, 2013, **135**(11), 4179–4182.
- 24 J. Li, S. Wu, C. Wu, L. Qiu, G. Zhu, C. Cui, Y. Liu, W. Hou, Y. Wang, L. Zhang, I. T. Teng, H. H. Yang and W. Tan, Versatile Surface Engineering of Porous Nanomaterials with Bioinspired Polyphenol Coatings for Targeted and Controlled Drug Delivery, *Nanoscale*, 2016, **8**(16), 8600–8606.
- 25 T. S. Sileika, D. G. Barrett, R. Zhang, K. H. Lau and P. B. Messersmith, Colorless Multifunctional Coatings Inspired by Polyphenols Found in Tea, Chocolate, and Wine, *Angew. Chem., Int. Ed.*, 2013, **52**(41), 10966–10970.
- 26 S. Quideau, D. Deffieux, C. Douat-Casassus and L. Pouysegur, Plant Polyphenols: Chemical Properties, Biological Activities, and Synthesis, *Angew. Chem., Int. Ed.*, 2011, **50**(3), 586–621.
- 27 Z. Chen, C. Wang, H. Zhou, L. Sang and X. Li, Modulation of Calcium Oxalatecrystallization by Commonly Consumed Green Tea, *CrystEngComm*, 2010, **12**(3), 845–852.
- 28 G. J. Du, Z. Zhang, X. D. Wen, C. Yu, T. Calway, C. S. Yuan and C. Z. Wang, Epigallocatechin Gallate (Egcg) Is the Most Effective Cancer Chemopreventive Polyphenol in Green Tea, *Nutrients*, 2012, **4**(11), 1679–1691.
- 29 I. Rady, H. Mohamed, M. Rady, I. A. Siddiqui and H. Mukhtar, Cancer Preventive and Therapeutic Effects of Egcg, the Major Polyphenol in Green Tea, *Egyptian Journal of Basic and Applied Sciences*, 2018, **5**(1), 1–23.
- 30 R. L. Pastore and P. Fratellone, Potential Health Benefits of Green Tea (*Camellia Sinensis*): A Narrative Review, *Explore*, 2006, **2**(6), 531–539.
- 31 T. Cheng, J. Liu, J. Ren, F. Huang, H. Ou, Y. Ding, Y. Zhang, R. Ma, Y. An, J. Liu and L. Shi, Green Tea Catechin-Based Complex Micelles Combined with Doxorubicin to Overcome Cardiotoxicity and Multidrug Resistance, *Theranostics*, 2016, **6**(9), 1277–1292.
- 32 Y. Peng, Q. Meng, J. Zhou, B. Chen, J. Xi, P. Long, L. Zhang and R. Hou, Nanoemulsion Delivery System of Tea Polyphenols Enhanced the Bioavailability of Catechins in Rats, *Food Chem.*, 2018, **242**, 527–532.
- 33 Z. Yi, Z. Sun, G. Chen, H. Zhang, X. Ma, W. Su, X. Cui and X. Li, Size-Controlled, Colloidally Stable and Functional Nanoparticles Based on the Molecular Assembly of Green Tea Polyphenols and Keratins for Cancer Therapy, *J. Mater. Chem. B*, 2018, **6**(9), 1373–1386.
- 34 J. Zhang, X. Ren, X. Tian, P. Zhang, Z. Chen, X. Hu and X. Mei, Gsh and Enzyme Responsive Nanospheres Based on Self-Assembly of Green Tea Polyphenols and Bsa Used for Target Cancer Chemotherapy, *Colloids Surf., B*, 2019, **173**, 654–661.
- 35 Y. Liu, S. Hu, Y. Feng, P. Zou, Y. Wang, P. Qin, J. Yue, Y. Liang, H. Wang and L. Liu, Preparation of Chitosan-Epigallocatechin-3-O-Gallate Nanoparticles and Their Inhibitory Effect on the Growth of Breast Cancer Cells, *J. Innovative Opt. Health Sci.*, 2018, **11**(04), 1850018.
- 36 K. Liang, J. E. Chung, S. J. Gao, N. Yongvongsoontorn and M. Kurisawa, Highly Augmented Drug Loading and Stability of Micellar Nanocomplexes Composed of Doxorubicin and Poly(Ethylene Glycol)-Green Tea Catechin Conjugate for Cancer Therapy, *Adv. Mater.*, 2018, **30**(14), e1706963.
- 37 H. Zhang, Z. Yi, Z. Sun, X. Ma and X. Li, Functional Nanoparticles of Tea Polyphenols for Doxorubicin Delivery in Cancer Treatment, *J. Mater. Chem. B*, 2017, **5**(36), 7622–7631.
- 38 X. Wang, X. Li, X. Liang, J. Liang, C. Zhang, J. Yang, C. Wang, D. Kong and H. Sun, Ros-Responsive Capsules Engineered from Green Tea Polyphenol-Metal Networks for Anticancer Drug Delivery, *J. Mater. Chem. B*, 2018, **6**(7), 1000–1010.
- 39 T. Liu, M. Zhang, W. Liu, X. Zeng, X. Song, X. Yang, X. Zhang and J. Feng, Metal Ion/Tannic Acid Assembly as a Versatile Photothermal Platform in Engineering Multimodal Nanotheranostics for Advanced Applications, *ACS Nano*, 2018, **12**(4), 3917–3927.
- 40 P. Y. Liu, Z. H. Miao, K. Li, H. Yang, L. Zhen and C. Y. Xu, Biocompatible Fe(3+)-Ta Coordination Complex with High Photothermal Conversion Efficiency for Ablation of Cancer Cells, *Colloids Surf., B*, 2018, **167**, 183–190.
- 41 J. E. Chung, S. Tan, S. J. Gao, N. Yongvongsoontorn, S. H. Kim, J. H. Lee, H. S. Choi, H. Yano, L. Zhuo, M. Kurisawa and J. Y. Ying, Self-Assembled Micellar Nanocomplexes Comprising Green Tea Catechin Derivatives and

- Protein Drugs for Cancer Therapy, *Nat. Nanotechnol.*, 2014, **9**(11), 907–912.
- 42 Y. Jia and J. Li, Molecular Assembly of Schiff Base Interactions: Construction and Application, *Chem. Rev.*, 2015, **115**(3), 1597–1621.
- 43 J. Wei, G. Wang, F. Chen, M. Bai, Y. Liang, H. Wang, D. Zhao and Y. Zhao, Sol-Gel Synthesis of Metal-Phenolic Coordination Spheres and Their Derived Carbon Composites, *Angew. Chem., Int. Ed.*, 2018, **57**(31), 9838–9843.
- 44 S. Honary and F. Zahir, Effect of Zeta Potential on the Properties of Nano-Drug Delivery Systems – a Review (Part 2), *Trop. J. Pharm. Res.*, 2013, **12**(2), 265–273.
- 45 Y. Dai, Z. Yang, S. Cheng, Z. Wang, R. Zhang, G. Zhu, Z. Wang, B. C. Yung, R. Tian, O. Jacobson, C. Xu, Q. Ni, J. Song, X. Sun, G. Niu and X. Chen, Toxic Reactive Oxygen Species Enhanced Synergistic Combination Therapy by Self-Assembled Metal-Phenolic Network Nanoparticles, *Adv. Mater.*, 2018, **30**(8), 1704877.
- 46 B. J. Kim, S. Han, K. B. Lee and I. S. Choi, Biphasic Supramolecular Self-Assembly of Ferric Ions and Tannic Acid across Interfaces for Nanofilm Formation, *Adv. Mater.*, 2017, **29**(28), 1700784.
- 47 J. H. Park, S. Choi, H. C. Moon, H. Seo, J. Y. Kim, S. P. Hong, B. S. Lee, E. Kang, J. Lee, D. H. Ryu and I. S. Choi, Antimicrobial Spray Nanocoating of Supramolecular Fe(III)-Tannic Acid Metal–Organic Coordination Complex: Applications to Shoe Insoles and Fruits, *Sci. Rep.*, 2017, **7**(1), 6980.
- 48 M. A. Rahim, M. Bjornmalm, N. Bertleff-Zieschang, Y. Ju, S. Mettu, M. G. Leeming and F. Caruso, Multiligand Metal-Phenolic Assembly from Green Tea Infusions, *ACS Appl. Mater. Interfaces*, 2018, **10**(9), 7632–7639.
- 49 W. Zhu, G. Xiang, J. Shang, J. Guo, B. Motevalli, P. Durfee, J. O. Agola, E. N. Coker and C. J. Brinker, Versatile Surface Functionalization of Metal–Organic Frameworks through Direct Metal Coordination with a Phenolic Lipid Enables Diverse Applications, *Adv. Funct. Mater.*, 2018, **28**(16), 1705274.
- 50 C. Yang, H. Wu, J. Shi, X. Wang, J. Xie and Z. Jiang, Preparation of Dopamine/Titania Hybrid Nanoparticles through Biomimetic Mineralization and Titanium(IV)-Catecholate Coordination for Enzyme Immobilization, *Ind. Eng. Chem. Res.*, 2014, **53**(32), 12665–12672.
- 51 M. A. Rahim, K. Kempe, M. Müllner, H. Ejima, Y. Ju, M. P. van Koeverden, T. Suma, J. A. Braunger, M. G. Leeming, B. F. Abrahams and F. Caruso, Surface-Confining Amorphous Films from Metal-Coordinated Simple Phenolic Ligands, *Chem. Mater.*, 2015, **27**(16), 5825–5832.
- 52 T. Zeng, X. Zhang, Y. Guo, H. Niu and Y. Cai, Enhanced Catalytic Application of Au@Polyphenol-Metal Nanocomposites Synthesized by a Facile and Green Method, *J. Mater. Chem. A*, 2014, **2**(36), 14807.
- 53 F. Ai, Q. Ju, X. Zhang, X. Chen, F. Wang and G. Zhu, A Core-Shell-Shell Nanoplatform Upconverting near-Infrared Light at 808 nm for Luminescence Imaging and Photodynamic Therapy of Cancer, *Sci. Rep.*, 2015, **5**, 10785.
- 54 H. Ejima, J. J. Richardson, K. Liang, J. P. Best, M. P. van Koeverden, G. K. Such, J. Cui and F. Caruso, One-Step Assembly of Coordination Complexes for Versatile Film and Particle Engineering, *Science*, 2013, **341**(6142), 154–157.
- 55 Y. Ping, J. Guo, H. Ejima, X. Chen, J. J. Richardson, H. Sun and F. Caruso, Ph-Responsive Capsules Engineered from Metal-Phenolic Networks for Anticancer Drug Delivery, *Small*, 2015, **11**(17), 2032–2036.
- 56 H. Liang, J. Li, Y. He, W. Xu, S. Liu, Y. Li, Y. Chen and B. Li, Engineering Multifunctional Films Based on Metal-Phenolic Networks for Rational Ph-Responsive Delivery and Cell Imaging, *ACS Biomater. Sci. Eng.*, 2016, **2**(3), 317–325.
- 57 E. Blanco, H. Shen and M. Ferrari, Principles of Nanoparticle Design for Overcoming Biological Barriers to Drug Delivery, *Nat. Biotechnol.*, 2015, **33**(9), 941–951.
- 58 M. Jurikova, L. Danihel, S. Polak and I. Varga, Ki67, PcnA, and Mcm Proteins: Markers of Proliferation in the Diagnosis of Breast Cancer, *Acta Histochem.*, 2016, **118**(5), 544–552.
- 59 Y. F. Yao, X. Liu, W. J. Li, Z. W. Shi, Y. X. Yan, L. F. Wang, M. Chen and M. Y. Xie, (–)-Epigallocatechin-3-Gallate Alleviates Doxorubicin-Induced Cardiotoxicity in Sarcoma 180 Tumor-Bearing Mice, *Life Sci.*, 2017, **180**, 151–159.